



Photocatalytic reduction of CO₂ to CO over the Ti–Highly dispersed HZSM-5 zeolite containing Fe

Yuecong Tong, Lu Chen, Shangbo Ning, Na Tong, Zizhong Zhang*, Huaxiang Lin, Fuying Li, Xuxu Wang*

State Key Laboratory of Photocatalysis on Energy and Environment, Fuzhou University, Fuzhou 350002, PR China



ARTICLE INFO

Article history:

Received 1 September 2016

Received in revised form 21 October 2016

Accepted 23 October 2016

Available online 24 October 2016

Keywords:

CO₂ photoreduction

HZSM-5

Fe–O species

Ti–O species

Semiconductor coupling

ABSTRACT

Iron-containing HZSM-5 zeolite, which was shown as an efficient and stable photocatalyst for photocatalytic CO₂ reduction in our previous research, was chosen to prepare a Ti–HZSM-5 hybrid via sol-gel method. The characterizations by XRD, UV-vis DRS, Raman, and XPS demonstrate that Ti species highly dispersed as nanoclusters or mono-sites on the HZSM-5 zeolite surface. Compared with the common TiO₂–HZSM-5 composite sample, the as-prepared Ti–HZSM-5 sample exhibits an enhanced activity for photocatalytic CO₂ reduction due to higher concentration of excited state electrons and faster electron transfer rate. The Ti–HZSM-5 sample with 0.99 wt% of Ti content is observed to have the highest rate for the photocatalytic CO₂ reduction. And the characterization results of photocurrent and ESR reveal that Ti species and Fe species work synergistically upon UV-light irradiation, therefore, we propose a possible reaction mechanism of CO₂ photoreduction on Ti–HZSM-5. This work highlights the promising prospect of hybridizing of the Fe–O species in zeolite with semiconductors for enhanced photocatalytic performance.

© 2016 Elsevier B.V. All rights reserved.

1. Introduction

The excessive utilization of fossil fuels is accompanied by emissions of large amounts CO₂. The increase in CO₂ emissions contributes to the increase in global temperatures and climate changes due to the greenhouse effect. Thus, reducing CO₂ emissions and developing alternative renewable energy resources are two extensive and long-term tasks [1–3]. Since solar power is abundant, clean and renewable, the solar-driven reduction of CO₂ into chemicals and fuels has been considered as the most promising approach to address the problems of global warming and energy crisis [4,5]. Towards photocatalytic reduction of CO₂ into chemicals and fuels, plenty of semiconductor photocatalysts (such as TiO₂ [6,7], Zn₂GeO₄ [8,9], C₃N₄ [10], ZrO₂ [11], WO₃ [12], and ZnO [13]) have been developed for such applications. Among them, TiO₂ is widely used in CO₂ photoreduction process due to its comparatively stability, non-toxicity, and low cost. Nevertheless, the efficiency for photocatalytic CO₂ reduction on TiO₂ is very low.

To enhance the efficiency for photocatalytic CO₂ reduction on TiO₂, TiO₂ particles should be small enough to offer a high specific

surface area and a mountain of active sites by unit mass [14]. Many approaches have been developed to immobilize TiO₂ nanoparticles on quartz plates or mesoporous substrates for improving its surface area and the dispersion of TiO₂ nanoparticles. It was reported that the TiO₂ nanoparticles that anchored onto quartz plate exhibited a much higher photocatalytic activity than the bulk TiO₂ power [6]. Anpo et al. reported that the microporous surface of zeolite with highly dispersed TiO₂ on the surface showed higher photocatalytic CO₂ reduction activity than bulk TiO₂ power [15–17].

High rate of electron-hole recombination and low rate of charge transfer are reasons for the low photocatalytic efficiency of TiO₂ for the reaction. Semiconductor coupling is an effective method for improving the separation of photogenerated electron-hole. In various preparation approaches of composite photocatalysts, architecture of the heterojunction between the different semiconductors with matching band potentials is one of the most dynamic strategies. Zou and co-workers [10] found that the activity of composite photocatalyst g-C₃N₄/NaNbO₃ for photoreduction of CO₂ was higher than that of the nude g-C₃N₄ or the nude NaNbO₃. Our group constructed the Sn/TiO₂ and Ni/TiO₂ with molecular junction Ti–O–Sn [18] and Ti–O–Ni [19] on the interface by surface organometallic chemistry methods, which effectively improve the activity of TiO₂ for H₂ production.

* Corresponding authors.

E-mail addresses: z.zhang@fzu.edu.cn (Z. Zhang), xwang@fzu.edu.cn (X. Wang).

Silicoaluminato molecular sieves have had wide application in catalysis field. Anpo et al. found that introducing transition metal atoms could lead the molecular sieves to show photocatalytic activity, and suggested that the metal-oxygen units could be excited by UV irradiation to form the charge-transfer excited state $[M^{(n-1)+}-O^-]^*$ similar to the photogenerated electron-hole pair on a semiconductor [20]. In the present study, HZSM-5 zeolite was selected as a support of TiO_2 based on our previous findings that HZSM-5 containing impurity Fe showed excellent photocatalytic activity. A novel hybrid photocatalyst was successfully prepared by anchoring TiO_2 to the HZSM-5 zeolite containing iron species. It is found that the hybrid photocatalyst shows very high activity for the photocatalytic reduction of CO_2 than the nude TiO_2 and the nude HZSM-5 in the aqueous solution, and the activity of the 0.99Ti-HZSM-5 sample is superior to that of the 0.99Ti O_2 -HZSM-5 sample. The characterizations by XRD, Raman, UV-vis DRS, XPS and N_2 physical adsorption reveal that Ti species highly dispersed as nanoclusters or mono-sites on the HZSM-5 zeolite surface. By combination with the ESR and photocurrent results, a possible reaction mechanism is suggested for the CO_2 photoreduction over Ti-HZSM-5.

2. Experimental details

2.1. Materials

HZSM-5 (Si/Al = 38) was obtained from Nankai University, China. Anatase TiO_2 (99%, 5 nm APS power) was purchased from Alfa Aesar. Tetrabutyl titanate ($Ti(OC_3H_7)_4$) and *n*-propanol were acquired from Sinopharm Chemical Reagent Co. Ltd.

2.2. Catalyst preparation

Ti-HZSM-5 was synthesized by sol-gel hydrolysis of tetrabutyl titanate on the HZSM-5 zeolites substrate. In a typical preparation procedure, 500 mg of HZSM-5 and a certain amount of tetrabutyl titanate were added to 100 mL of *n*-propanol solution, and stirred for 2 h. Then an *n*-propanol solution with 10% water was added dropwise with a burette to the above solution under stirring condition during 3 h. The resulting gel solution was maintained in the same stirring condition for 2 h. The solid was centrifuged, washed several times with distilled water, then dried at 353 K followed by calcined at 773 K for 4 h. The as-synthesized samples were denoted as xTi-HZSM-5, where x represents the mass percentage of Ti in the sample. The sample prepared by mechanical mixing method was defined as xTi O_2 -HZSM-5, x indicated the mass percentage of Ti mixed with HZSM-5.

2.3. Characterization of physicochemical properties

X-ray diffraction (XRD) patterns were obtained using a Bruker D8 Advance X-ray diffractometer operated at 40 kV and 40 mA with Ni-filtered Cu $K\alpha$ irradiation ($\lambda = 0.15406$ nm). UV-vis diffuse reflectance spectra (DRS) were recorded on a Cary-500 UV-vis-NIR spectrometer, BaSO₄ powder was used as the internal standard. The content of Ti in the samples was measured by an inductively coupled plasma optical emission spectrometer (ICP-OES) (Ultima2, HORIBA Jobin Yvon). Raman spectra were recorded at room temperature using a confocal microscopy Raman spectrometer (inVia, Renishaw Co., Britain) in the backscattering geometry with a 532 nm diode laser as an excitation source. Nitrogen adsorption-desorption isotherms and CO_2 adsorption isotherms were measured respectively at 77 K and 273 K, with an ASAP2020 M apparatus (Micromeritics Instrument Corp., USA). Brunauer–Emmett–Teller (BET) surface areas of samples were calculated from the N_2 adsorption isotherm by standard method.

X-ray photoelectron spectroscopy (XPS) measurements were conducted on a PHI Quantum 2000 XPS system equipped with an Al X-ray source (1486.6 eV). Electron spin resonance (ESR) spectra were measured by a Bruker A-300-EPR X-band spectrometer at 77 K.

Photoelectrochemical measurements were conducted with a BAS Epsilon Electrochemical System in a conventional three electrode cell, using a Pt plate as the counter electrode and Ag/AgCl electrode (3 M KCl) as the reference electrode. The working electrode was prepared by cleaning a fluorine-doped tin oxide (FTO) glass. The photocatalyst was dispersed in ethanol, and the suspension was added dropwise directly onto 0.25 cm² of FTO glass substrate. Then the film was dried in air. The electrochemical measurement was carried out in a Na₂SO₄ (0.2 M) electrolyte, which was purged with nitrogen gas for 2 h prior to the measurements.

2.4. Characterization of photocatalytic activity

Photocatalytic reduction of CO_2 was conducted in a 40 mL quartz reactor with a silicone rubber septum. 1 mL of CO_2 -saturated aqueous solution, which had been prepared by bubbling with high purity CO_2 (99.999%) gas to 5 mL H₂O for 30 min, was added into the quartz reactor with 20 mg of catalyst. To remove air from the reactor and prevent water extraction, the reactor was cooled by an ice-water bath to 273 K, then evacuated by a mechanical pump and filled with high purity CO_2 gas. The evacuation-filling operation was repeated three times. A 300 W commercial Xe lamp was used as an irradiation resource and vertically placed outside the reactor. The temperature of the reactor was kept at room temperature with an electronic fan. And the reaction mixture was stirred with a magnetic stirrer during the whole reaction process. After 3 h of irradiation, 0.5 mL of reactive gas was sampled with a syringe after different reaction time, and analyzed by a GC-7890B gas chromatograph equipped with a flame ionization detector (FID), a thermal conductivity detector (TCD) and a methanation reactor which can convert CO and CO_2 to CH₄. The incident light intensity of Xe lamp was measured by using a SpectriLight ILT950 (Fig. S1). The Xe lamp has a continuous output spectrum in 330–800 nm and the main peak at ca. 410 nm.

3. Results and discussion

3.1. Photocatalytic activity of samples for CO_2 reduction

The photocatalytic reduction of CO_2 over the samples was performed under Xe lamp irradiation in the CO_2 -saturated aqueous solution without any sacrificial agent. CO was main product of the reaction, and beyond CO product, only a trace amount of CH₄ and H₂ was detected in the gas phase products. Fig. 1 shows the production rates of CO over the Ti-HZSM-5 samples with different Ti loading amount and the several reference samples such as the nude TiO_2 , the nude HZSM-5, and the 0.99Ti O_2 -HZSM-5. Obviously, the 0.99Ti-HZSM-5 sample shows the highest production rate of CO in all the samples, reaching to 2.05 $\mu\text{mol g}^{-1} \text{h}^{-1}$, which is 2.8 time higher than that of the 0.99Ti O_2 -HZSM-5. This indicates that the loading Ti species could increase the photocatalytic activity of both TiO_2 and HZSM-5 for reduction of CO_2 to CO. However, the sample obtained by sol-gel hydrolysis (0.99Ti-HZSM-5) shows higher activity than the sample by mechanical mixing (0.99Ti O_2 -HZSM-5). The difference of the samples in the photocatalytic activity should be related to the existence of Fe species in HZSM-5 and the chemical states of the introduced Ti species.

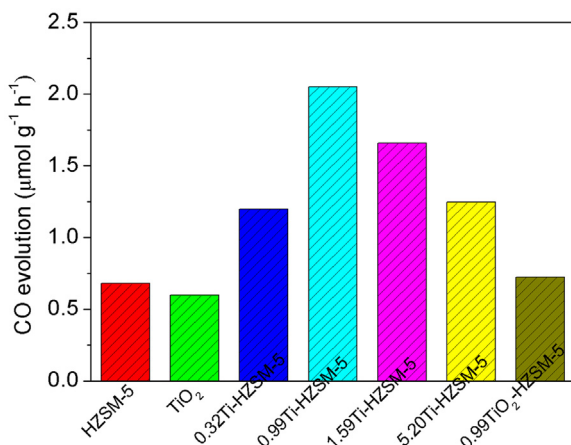


Fig. 1. CO production rates obtained for photocatalytic reduction of CO_2 by different catalysts.

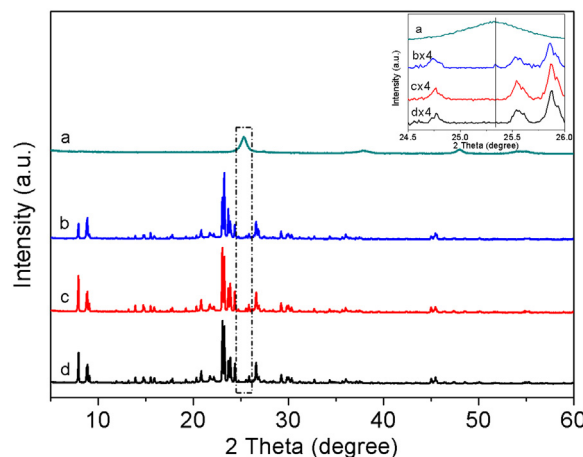


Fig. 2. XRD patterns of TiO_2 (anatase) (a), 0.99Ti₂-HZSM-5 (b), 0.99Ti-HZSM-5 (c), HZSM-5 (d).

3.2. Composition and structure characterizations of the catalysts

3.2.1. XRD analysis

Fig. 2 shows XRD patterns of the 0.99Ti-HZSM-5, 0.99Ti₂-HZSM-5 and two reference samples TiO_2 and HZSM-5. Compared with that of the nude HZSM-5 sample, the Ti-containing samples show no any change in the position of XRD diffraction peaks, suggesting the introduction of Ti species did not destroy the MFI-type crystal structure of HZSM-5. However, for the mechanically mixed sample, 0.99Ti₂-HZSM-5, relative intensities of the several main diffraction peaks seem to show notable change, and a small diffraction peak attributable to TiO_2 could be distinguished from the characteristic diffractions of HZSM-5 (see the inset in Fig. 2). This indicates heterogeneous dispersion of TiO_2 as small crystal particle over the pore surface of HZSM-5. By contrast, for the 0.99Ti-HZSM-5 sample, no any diffraction peak belonging to TiO_2 is observed, and the intensities of all diffraction peaks are almost comparable to that of the nude HZSM-5. This indicates that Ti species are highly dispersed on pore surface of HZSM-5 for 0.99Ti-HZSM-5.

3.2.2. Raman spectra

Visible Raman spectroscopy is sensitive to TiO_2 but not to HZSM-5 [21], which was further applied to ascertain the difference in the chemical state of Ti species of these HZSM-5 samples. As shown in Fig. 3, TiO_2 (anatase) exhibits four Raman bands at 144, 390, 516, and 637 cm^{-1} , which are completely consistent with those

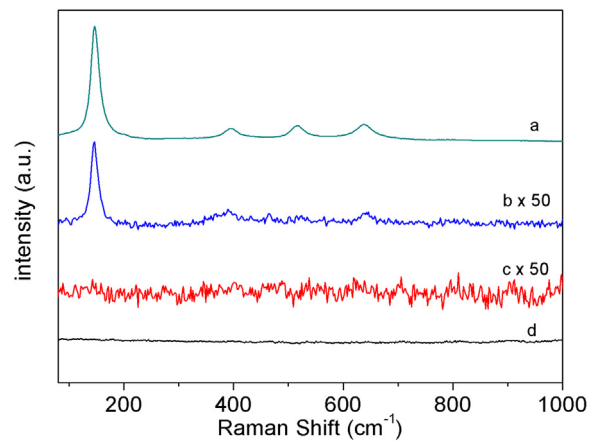


Fig. 3. Raman patterns ($\lambda_{\text{ex}} = 532\text{ nm}$) of TiO_2 (anatase) (a), 0.99Ti₂-HZSM-5 (b), 0.99Ti-HZSM-5 (c) and HZSM-5 (d).

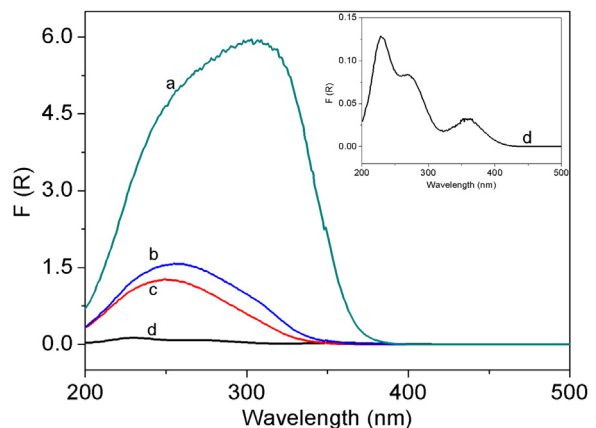


Fig. 4. UV-vis diffuse reflectance spectra of TiO_2 (anatase) (a), 0.99Ti₂-HZSM-5 (b), 0.99Ti-HZSM-5 (c) and HZSM-5 (d).

reported in the literatures [22,23]. The observed axial signal for 0.99Ti₂-HZSM-5 is similar to the corresponding signal observed for TiO_2 (anatase). But no any Raman adsorption bands related to TiO_2 is found for the 0.99Ti-HZSM-5 sample. The Raman result supports the XRD result that the titanium oxide species can present as anatase phase nanoparticle in the 0.99Ti₂-HZSM-5 samples, while present as a high disperse state in the 0.99Ti-HZSM-5 sample [24].

3.2.3. DRS spectra

It is well known that the UV absorption bands are a result of the ligand-to-metal charge transfer for metal oxides, and therefore it can be used to characterize the coordination chemistry of the metal ions in the materials containing metal species. Fig. 4 is UV-vis diffuse reflectance spectra (DRS) of these samples. The nude anatase TiO_2 shows a wide absorption band with the biggest absorption at ca. 310 nm and a ca. 380 nm of absorption edges. Such wide absorption profile is completely in accord with that of the TiO_2 nanocrystals reported in literature, indicating diversity of the chemistry states of Ti atom in the TiO_2 nanocrystals. The nude HZSM-5 shows very weak DRS absorption feature compared to the TiO_2 , but it has actually three peaks in the range of 200–500 nm (see the inset in Fig. 4), the two bands at ca. 220 and 280 nm are assigned to the charge transfer from ligand to isolated framework Fe^{3+} , and the band at ca. 360 nm is related to d-d electron transition of Fe^{3+} in tetrahedral symmetry [25,26]. Weaker UV peaks of the HZSM-5 could be due to lower content and lower absorption

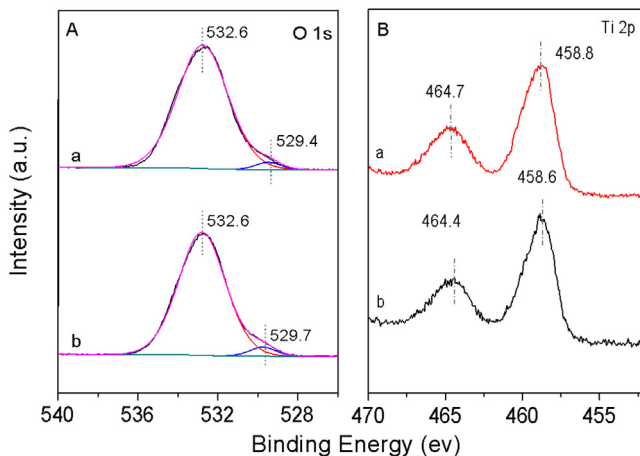


Fig. 5. High-resolution XPS spectra of the O1s (A) and Ti2p (B) of 0.99TiO₂-HZSM-5 (a) and 0.99Ti-HZSM-5 (b).

coefficient of Fe-O species than those of Ti-O species. Compared to the nude anatase TiO₂, both the 0.99TiO₂-HZSM-5 and the 0.99Ti-HZSM-5 show narrower absorption band, and the absorption edges of them are shifted toward short wavelength. Interestingly, the absorption band of 0.99Ti-HZSM-5 is narrower and the absorption wavelength of absorption edge is shorter. Since the absorption wavelength of metal atom is generally blue-shifted with decreasing coordination number of it [27], the DRS characterization suggests that the Ti atoms in the 0.99Ti-HZSM-5 should be mainly present as the Ti species with lower coordination numbers [24,28], while those in the 0.99TiO₂-HZSM-5 should be present as the TiO₂ nanoparticles [29,30], which is agreed well with XRD and Raman results.

3.2.4. XPS characterization

X-ray Photoelectron Spectroscopy (XPS) was used to further characterize the difference in the chemical states of Ti species in two Ti-containing HZSM-5 materials. O1s and Ti2p photoelectron spectra of the samples are shown in Fig. 5. The O1s spectrum could be deconvolved into two peaks. The one at higher binding energy is attributed to the oxygen atom of HZSM-5 [31], and the other one at lower binding energy is belonged to the oxygen atom of TiO₂ [32]. Compared with those of 0.99TiO₂-HZSM-5, the O1s peak at high energy of the 0.99Ti-HZSM-5 shows almost unchanged, while O1s peak of 0.99Ti-HZSM-5 at low energy shifts ca. 0.3 eV toward high binding energy. This shows that the oxygen atoms in the 0.99Ti-HZSM-5 sample have lower electron density than those in 0.99TiO₂-HZSM-5. In contrast, the Ti2p_{3/2} and Ti2p_{1/2} binding energies of 0.99Ti-HZSM-5 sample shift ca. 0.2 eV toward low binding energy, compared to that of 0.99TiO₂-HZSM-5 sample. The results suggest that there are more electrons transfer from O to Ti in the 0.99Ti-HZSM-5 than in the 0.99TiO₂-HZSM-5. This indicates that polarizability of Ti—O bond occurs for the surface of 0.99Ti-HZSM-5 sample, which could be explained by the Ti species bonded chemically to the surface of HZSM-5. Our previous studies show that the HZSM-5 sample contains very low content of Fe (ca 0.03 wt%) [26], this content is too low to be clearly detected by XPS.

All the above results show that the 0.99Ti-HZSM-5 has chemical states of Ti species different from the 0.99TiO₂-HZSM-5. On the 0.99Ti-HZSM-5 surface, the Ti atoms could bond to the surface of HZSM-5 by O bridge, and therefore has strong interaction with the surface Fe species, which can be essential reason for higher activity of 0.99Ti-HZSM-5 than 0.99TiO₂-HZSM-5.

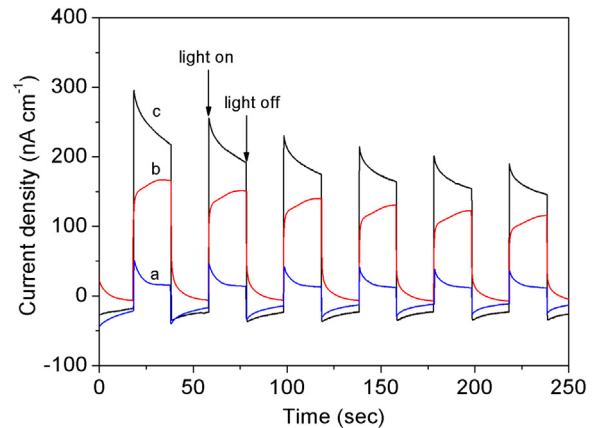


Fig. 6. Periodic on/off photocurrent response of HZSM-5 (a), 0.99TiO₂-HZSM-5 (b) and 0.99Ti-HZSM-5 (c) electrodes in 0.2 M Na₂SO₄ electrolyte with zero bias versus Ag/AgCl.

3.3. Texture of samples

Texture data of the HZSM-5 and the Ti-containing HZSM-5 samples were measured by the N₂ adsorption, as listed in Table 1. It can be seen that both the specific surface areas and pore diameter of 0.99TiO₂-HZSM-5 sample are slightly lower than that of the HZSM-5, which may be due to the pores of HZSM-5 partly blocking by TiO₂ particles. In contrast, the specific surface areas of 0.99Ti-HZSM-5 sample is a bit higher than that of the HZSM-5, but its pore diameter is a bit lower than the HZSM-5, which could be understood also by the chemical bonding of Ti species to surface oxygen atoms of TiO₂. It should be noted that such a small change of specific surface area and pore size could not induce such a difference in the photocatalytic activity between Ti-HZSM-5 and TiO₂-HZSM-5, which could be seen from the normalized rates on the two samples. Thus, specific surface area and CO₂ adsorption capacity are not responsible for the difference in photocatalytic activity.

3.4. Photocurrent under UV light

Fig. 6 shows the photocurrent response of the samples. The 0.99Ti-HZSM-5 sample exhibits the higher photocurrent than the 0.99TiO₂-HZSM-5 and HZSM-5 samples, indicating that 0.99Ti-HZSM-5 catalyst possesses higher efficiency of the separation of photogenerated electron-hole pairs than the other samples.

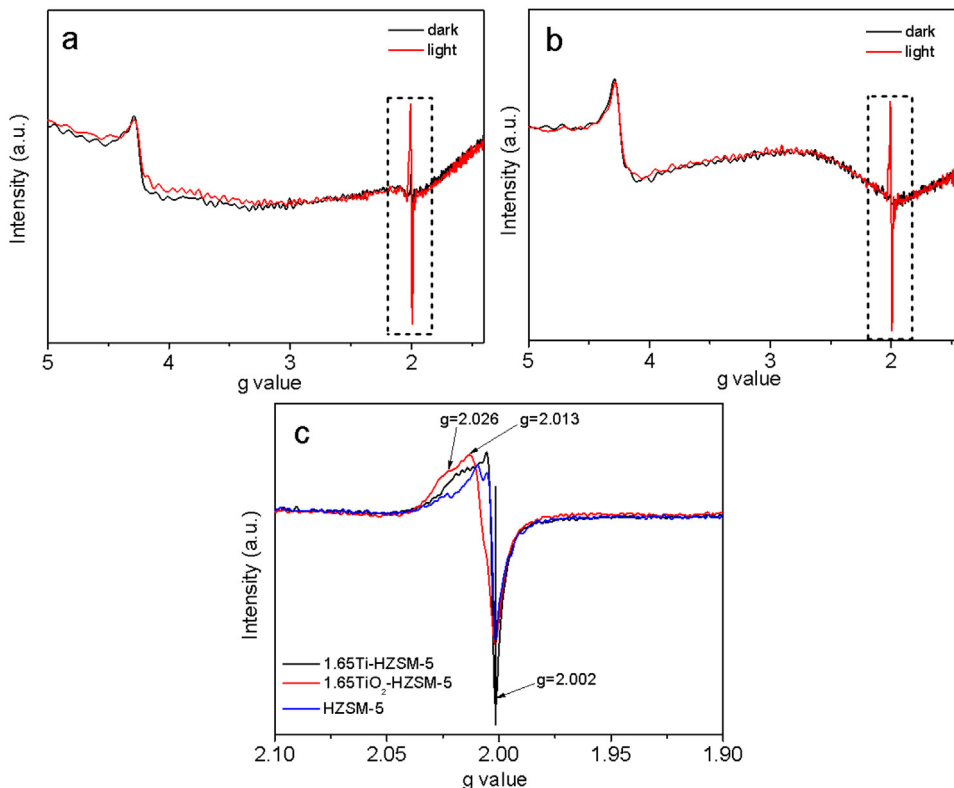
3.5. ESR characterization

Electron spin resonance (ESR) spectroscopy was used to explore the electron transfer process during UV light irradiation over HZSM-5 and Ti-containing HZSM-5 catalysts. The ESR experiments were carried out at 77 K in order to slow down the rate of electron transfer. According to Fig. 7a and b, both the 0.99TiO₂-HZSM-5 and the 0.99Ti-HZSM-5 show two wide ESR signals at $g = 4.27$ and $g = 2.026\text{--}2.002$, of which the former is attributed to Fe³⁺ [33–35], and the latter to O[·] species [29,36–40]. No Ti³⁺ signal is detected for two samples. For clearly, Fig. 7c shows amplifying ESR signals at $g = 2.026\text{--}2.002$. The signal at $g = 2.002$ can be attributed to O[·] species of Fe—O [40,41], and the ones at 2.013 and 2.026 can be assigned to O[·] species of Ti—O—Ti [36,37]. Significantly, for the 0.99TiO₂-HZSM-5, upon irradiation the signal intensity of Fe³⁺ is slightly decreased, but the signal of O[·] species ($g = 2.026\text{--}2.002$) is considerably increased, implying that UV excitation lead to an electron transfer from O²⁻ to Ti⁴⁺ and to Fe³⁺ to form [Ti³⁺—O[·]]^{*} and [Fe²⁺—O[·]]^{*} over the 0.99TiO₂-HZSM-5, respectively. But for 0.99Ti-HZSM-5, upon the UV irradiation, the intensity of Fe³⁺ signal keeps

Table 1

Comparison of the physical properties and photocatalytic activity of different sample.

Samples	BET surface area ($\text{m}^2 \text{ g}^{-1}$)	Mean pore diameter (nm)	$A(\text{CO}_2)$ ($\text{cm}^3 \text{ g}^{-1}$) ^a	$R_{\text{CO}} * 10^{-3}$ ($\mu\text{mol h}^{-1} \text{ m}^{-2}$) ^b	R'_{CO} ($\mu\text{mol h}^{-1} \text{ cm}^{-3}$) ^c
HZSM-5	277.6	0.534	48.3	2.45	0.014
0.99Ti-HZSM-5	281.5	0.529	47.1	7.28	0.044
0.99TiO ₂ -HZSM-5	263.9	0.526	45.8	2.61	0.016

^a Adsorbed capacity of CO₂.^b Production rate of CO normalized with specific surface areas.^c Production rate of CO normalized with CO₂ adsorbed capacity.**Fig. 7.** ESR spectra of 0.99TiO₂-HZSM-5 (a) and 0.99Ti-HZSM-5 (b) under dark at 77 K in vacuum. (c) the selected region ESR spectra of the 0.99TiO₂-HZSM-5 (red), 0.99Ti-HZSM-5 (black) and HZSM-5 (blue) samples upon UV light irradiation. (For interpretation of the references to colour in this figure legend, the reader is referred to the web version of this article.)

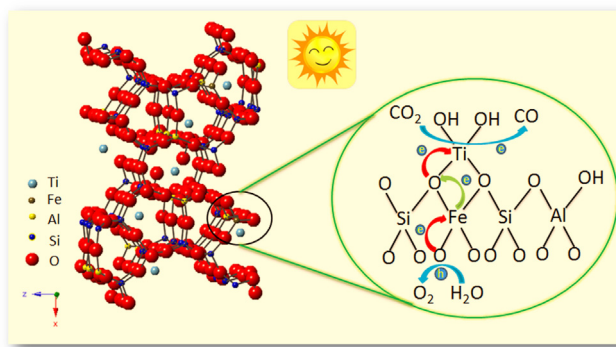
almost constant in the same condition, and for the signal of O[−] species, in addition to a weak signal ($g = 2.026$) assigned to the O atoms in Ti–O–Ti, signal location of O[−] species in 0.99Ti-HZSM-5 is essentially consistent with that in HZSM-5, indicating most O[−] species present in the Fe–O. The above results suggest that upon irradiation, the photogenerated electrons of [Fe²⁺–O[−]]^{*} species can transfer to the O[−] species of [Ti³⁺–O[−]]^{*} for the 0.99Ti-HZSM-5. And stronger signal of O[−] species is observed on 0.99Ti-HZSM-5 under UV light irradiation, indicating that photogenerated electrons transfer from [Fe²⁺–O[−]]^{*} species to O[−] species of [Ti³⁺–O[−]]^{*} is beneficial to promote charge separation. The result is well agreed with the experimental data of photocurrent. Therefore, the enhancement of the photocatalytic performance over Ti-HZSM-5 can be well explained based on the above experimental results and analysis.

3.6. Photocatalytic mechanism

The above results show that dependent on the introduction mode of Ti species, the resulting Ti-contained HZSM-5 samples show notable difference in the chemical states, texture, photocurrent response, and photoexcitation property. By combining with

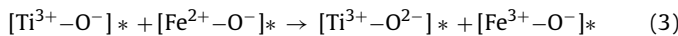
our previous data on the characterization for Fe species of HZSM-5, we suggest possible mechanism of photocatalytic reduction of CO₂ on the Ti-HZSM-5 in aqueous solution.

The used HZSM-5 sample was characterized to contain ca 0.03 wt% of Fe and the Fe atoms are present as tetrahedrally coordinated Fe-O species incorporated within the silica framework [26]. When introduced of Ti species by sol-gel hydrolysis of tetrabutyl titanate on the HZSM-5, the Ti species is anchored to the HZSM-5 surface by coordination with the framework oxygen atoms. Because the Ti species and Fe species coexist on the surface of HZSM-5, the Fe–O and Ti–O excited states would be formed simultaneously when the sample is irradiated by UV light. The enhancement of photocatalytic performance over Ti-HZSM-5 sample is related closely to the coupling effect between the two excited states. The coupling would lead to increase in the concentration of excited electrons and acceleration of the electron transfer rate over Ti-HZSM-5. The possible mechanism of the CO₂ photoreduction over Ti-HZSM-5 is showed in Scheme 1. Firstly, CO₂ and H₂O molecules are adsorbed on Ti-HZSM-5 surface as weak ligands to form the reaction precursors. Upon UV light irradiation, [Fe³⁺–O^{2−}] and [Ti⁴⁺–O^{2−}] species would be excited to form [Fe²⁺–O[−]]^{*} and [Ti³⁺–O[−]]^{*} species simultaneously, then photogenerated electrons of [Fe²⁺–O[−]]^{*} species



Scheme 1. The possible mechanism for photoreduction of CO_2 with H_2O on Ti-HZSM-5 composite.

quickly transfer to O^- species of $[\text{Ti}^{3+}-\text{O}^-]^*$, which facilitates the separation and migration of photoexcited electrons.



Finally, CO_2 is reduced to CO by $[\text{Ti}^{3+}-\text{O}^{2-}]$ species and H_2O is oxidized to O_2 by $[\text{Fe}^{3+}-\text{O}^-]$ species. Reduction and oxidation reaction occurring at different photoactive center would decrease electron-hole recombination and reverse reaction.

4. Conclusion

In summary, Ti atoms are successfully anchored on HZSM-5 zeolite containing iron species via an in situ loading method. The combined characterizations of Ti-HZSM-5 by XRD, UV-vis DRS, Raman and XPS demonstrate that in the as-synthesized Ti-HZSM-5 sample, Ti species are highly dispersed as lower coordination state on HZSM-5 zeolite surface, which makes Ti species and Fe species work synergistically. Such a surface feature enhances separation efficiency of the photogenerated electron-hole pairs. The Ti-HZSM-5 composite shows higher photocatalytic activity for CO_2 reduction to CO than the TiO_2 -HZSM-5 sample. Our work provides an effective method in direct constructing semiconductor/zeolite photocatalyst composite, which can effectively enhance the photocatalytic activity of the catalyst. This synthetic approach is expected to extend to the production of other heterojunction zeolite photocatalysts.

Acknowledgements

The work is financially supported by the National Natural Science Foundation of China (Grants No. U1305242), the Technology Project of Education Office of Fujian Province of PR China (JA14030) and Collaborative Innovation Center of Clean Coal Gasification Technology of Fujian (No. XK1401).

Appendix A. Supplementary data

Supplementary data associated with this article can be found, in the online version, at <http://dx.doi.org/10.1016/j.apcatb.2016.10.065>.

References

- [1] V.M. Malhotra, *Concr. Int.* 28 (2006) 42–45.
- [2] T.R. Cook, D.K. Dogutan, S.Y. Reece, Y. Surendranath, T.S. Teets, D.G. Nocera, *Chem. Rev.* 110 (2010) 6474–6502.
- [3] S. Günes, H. Neugebauer, N.S. Sariciftci, *Chem. Rev.* 107 (2007) 1324–1338.
- [4] N.S. Lewis, D.G. Nocera, *Proc. Natl. Acad. Sci.* 103 (2006) 15729–15735.
- [5] S.N. Haberreuter, L. Schmidt-Mende, J.K. Stolarczyk, *Angew. Chem. Int. Ed.* 52 (2013) 7372–7408.
- [6] S. Neatu, J.A. Macia-Agullo, P. Concepcion, H. Garcia, *J. Am. Chem. Soc.* 136 (2014) 15969–15976.
- [7] Q. Zhai, S. Xie, W. Fan, Q. Zhang, Y. Wang, W. Deng, Y. Wang, *Angewandte Chemie* 52 (2013) 5776–5779.
- [8] L. Qi, Z. Yong, K. Jiahui, C. Xiaoyu, T. Zhongping, G. Jun, Y. Shicheng, Z. Zhigang, *J. Am. Chem. Soc.* 132 (2010) 14385–14387.
- [9] Q. Liu, Y. Zhou, Z. Tian, X. Chen, J. Gao, Z. Zou, *J. Mater. Chem.* 22 (2012) 2033.
- [10] H. Shi, G. Chen, C. Zhang, Z. Zou, *ACS Catal.* 4 (2014) 3637–3643.
- [11] Y. Kohno, T. Tanaka, T. Funabiki, S. Yoshida, *Phys. Chem. Chem. Phys.* 2 (2000) 2635–2639.
- [12] X. Chen, Y. Zhou, Q. Liu, Z. Li, J. Liu, Z. Zou, *ACS Appl. Mater. Interfaces* 4 (2012) 3372–3377.
- [13] G. Mahmodi, S. Sharifnia, M. Madani, V. Vatanpour, *Sol. Energy* 97 (2013) 186–194.
- [14] Z. Zhang, C.-C. Wang, R. Zakaria, J.Y. Ying, *J. Phys. Chem. B* 102 (1998) 10871–10878.
- [15] M. Anpo, H. Yamashita, Y. Ichihashi, Y. Fujii, M. Honda, *J. Phys. Chem. B* 101 (1997) 2632–2636.
- [16] K. Ikeue, H. Yamashita, M. Anpo, T. Takewaki, *J. Phys. Chem. B* 105 (2001) 8350–8355.
- [17] M. Anpo, H. Yamashita, K. Ikeue, Y. Fujii, S.G. Zhang, Y. Ichihashi, D.R. Park, Y. Suzuki, K. Koyano, T. Tatsumi, *Catal. Today* 44 (1998) 327–332.
- [18] Q. Gu, J. Long, Y. Zhou, R. Yuan, H. Lin, X. Wang, *J. Catal.* 289 (2012) 88–99.
- [19] L. Fan, J. Long, Q. Gu, H. Huang, H. Lin, X. Wang, *J. Catal.* 320 (2014) 147–159.
- [20] M. Matsuoka, M. Anpo, *J. Photochem. Photobiol. C Photochem. Rev.* 3 (2003) 225–252.
- [21] C. Li, G. Xiong, J. Liu, P. Ying, Q. Xin, Z. Feng, *J. Phys. Chem. B* 105 (2001) 2993–2997.
- [22] T. Ohnsaka, F. Izumi, Y. Fujiki, *J. Raman Spectrosc.* 7 (1978) 321–324.
- [23] R.B. Quincy, M. Houalla, D.M. Hercules, *J. Catal.* 106 (1987) 85–92.
- [24] L. Li, P. Wu, Q. Yu, G. Wu, N. Guan, *Appl. Catal. B: Environ.* 94 (2010) 254–262.
- [25] S. Bordiga, R. Buzzoni, F. Geobaldo, C. Lamberti, E. Giannello, A. Zecchina, G. Leofanti, G. Petrini, G. Tozzola, G. Vlaic, *J. Catal.* 158 (1996) 486–501.
- [26] G. Yan, X. Wang, X. Fu, D. Li, *Catal. Today* 93–95 (2004) 851–856.
- [27] J. Klaas, A. Günter Schulzkeff, N.I. Jaeger, *J. Phys. Chem. B* 101 (1997) 1305–1311.
- [28] J. Zhang, Y. Hu, M. Matsuoka, H. Yamashita, M. Minagawa, H. Hidaka, M. Anpo, *J. Phys. Chem. B* 105 (2001) 8395–8398.
- [29] Z. Chang, L. Kevan, *Phys. Chem. Chem. Phys.* 4 (2002) 5649–5654.
- [30] M. Liu, X. Guo, X. Wang, C.-h. Liang, C. Li, *Catal. Today* 93 (2004) 659–664.
- [31] R.J. Davis, Z. Liu, *Chem. Mater.* 9 (1997) 2311–2324.
- [32] Q. Gu, J. Long, L. Fan, L. Chen, L. Zhao, H. Lin, X. Wang, *J. Catal.* 303 (2013) 141–155.
- [33] M. Nishikawa, Y. Mitani, Y. Nosaka, *J. Phys. Chem. C* 116 (2012) 14900–14907.
- [34] A.V. Kucherov, M. Shelef, *J. Catal.* 195 (2000) 106–112.
- [35] E.A. Zhilinskaya, G. Delahay, M. Mauvezin, B. Coq, A. Aboukaïs, *Langmuir* 19 (2003) 3596–3602.
- [36] O.I. Micic, Y. Zhang, K.R. Cromack, A.D. Trifunac, M.C. Thurnauer, *J. Phys. Chem.* 97 (1993) 7277–7283.
- [37] S. Zhang, N. Fujii, Y. Nosaka, *J. Mol. Catal. A: Chem.* 129 (1998) 219–224.
- [38] T. Berger, M. Sterrer, O. Diwald, E. Knözinger, D. Panayotov, T.L. Thompson, J.T. Yates, *J. Phys. Chem. B* 109 (2005) 6061–6068.
- [39] A.M. Prakash, S.S. And, L. Kevan, *J. Phys. Chem. B* 102 (1998).
- [40] H.-T. Sun, Y. Sakka, N. Shirahata, Y. Matsushita, K. Deguchi, T. Shimizu, *J. Phys. Chem. C* 117 (2013) 6399–6408.
- [41] Y. Tong, Y. Zhang, N. Tong, Z. Zhang, Y. Wang, X. Zhang, S. Zhu, F. Li, X. Wang, *Catal. Sci. Technol.* 6 (2016) 7579–7585.